Bulletin of Earthquake Engineering
https://doi.org/10.1007/s10518-024-01972-3

ORIGINAL ARTICLE

Minimum magnitude boundaries in probabilistic seismic hazard analysis: an insight from structural engineering

Alireza Azarbakht[1]

Received: 24 February 2024 / Accepted: 30 June 2024

Abstract

In order to systematically advance our understanding of the minimum magnitude limit (M_{min}) in the probabilistic seismic hazard analysis (PSHA) calculations, a novel and useful approach utilising a broad range of Single-Degree-of-Freedom oscillators and hazard conditions is being developed and tested. We have determined the most reasonable M_{min} value for a variety of structures by examining the impact of M_{min} on the mean annual frequency (MAF) of various limit states (LSs) (including the collapse capacity). The originality of the suggested methodology in the current work, known as the MAF saturation strategy, is the recommended M_{min}, which is the cut-off value at which lesser magnitude events do add to the hazard but do not significantly change the MAF. The current work is the first to offer the MAF saturation strategy methodology, which searches for the cut-off magnitude at which the MAF value essentially remains constant even when smaller values of this cut-off are utilised as M_{min} for hazard assessments. Therefore, given a series of carefully chosen ground motions in each oscillator instance, an incremental dynamic analysis is carried out (by applying the Hunt and Fill algorithm), and the appropriate LS (including the collapse capacity defined as global instability) points are calculated. Thus, the relationship between the distribution of LSs and the Engineering Demand Parameter and intensity measure is found. A simple point source hazard curve is convoluted with this distribution, yielding the structure-specific MAF. In order to find the cut-off lower magnitude (M_{min}), this convolution is repeated for several M_{min} values. This cut-off is defined as the point at which, when lower values are utilised as M_{min} in the PSHA computation, the MAF's values do not change considerably (with a five per cent threshold). The acquired data were thoroughly discussed in relation to various structural features and seismic input factors. The primary findings showed that each of the structures under consideration requires a M_{min} value in the range of 4–4.3. Put otherwise, the suggestions seen in technical literature, which range from 4.5 to 5, are not cautious, at least not when it comes to probabilistic structural limit state frequency. The derived M_{min} value is mostly controlled by the natural period of the structure and is largely unaffected by other structural characteristics like ductility, damping ratio and overstrength factor.

Keywords Performance-based earthquake engineering · Nuclear power plant · Mean annual frequency · Limit state · Incremental dynamic analysis · Numerical fragility · SDOF · MDOF · EDP · Near-field ground motion record

Extended author information available on the last page of the article

Published online: 09 July 2024

1 Introduction

PSHA is a crucial technique for determining the probability of different intensities of ground shaking at particular sites within a specified time frame. In order to make sure that both new and existing structures can resist potential seismic occurrences, this method is essential for influencing the design and safety assessments of those structures. PSHA assists engineers and decision-makers in creating efficient plans to reduce seismic hazards and improve the resilience of infrastructure by calculating the likelihood of various degrees of earthquake ground motion (Kramer 1996; McGuire 2004).

Integrating data on a region's seismicity, anticipated rates of earthquake occurrence, and possible ground shaking intensities is the fundamental idea of PSHA. Estimates of the annual frequency of surpassing different levels of ground motion are provided by the derived hazard curves. The creation of construction rules, the planning of vital infrastructure, and the execution of disaster readiness and response plans all depend on these hazard curves. PSHA has developed into a key component of earthquake engineering over time, advancing both risk management and structure design (Baker et al. 2021).

The Gutenberg-Richter (GR) law, which describes the frequency-magnitude distribution of earthquakes, is commonly used by PSHA. The frequency of lesser and moderate earthquakes is well captured by this model, which depicts a linear relationship between the logarithm of earthquake frequency and magnitude (Gutenberg and Richter 1955). Although the General Relativity (GR) model has been widely used and is empirically robust, it has significant shortcomings, especially when it comes to explaining the occurrence of large, rare earthquakes in areas with intricate fault networks (Schwartz and Coppersmith 1984; Wesnousky 1994). To overcome these restrictions, a number of substitute models have been put out to better represent the behaviour of huge earthquakes (Gerstenberger et al. 2020). Non-extensive statistical physics models, such as the one put forth by Sotolongo-Costa and Posadas (2004), have been offered more recently. These models provide a more thorough understanding of earthquake recurrence by taking into account the intricacies of fault systems and the interconnections between various seismic events.

A crucial PSHA parameter that establishes the lower bound for earthquake magnitudes taken into account in hazard assessments is the Minimum Magnitude (M_{min}). It restricts the spectrum of earthquakes that are included in the evaluation, which affects the seismic hazard calculation. Although minor earthquakes alone are less likely to result in major damage, their combined effect can be significant in some situations, especially for structures that are susceptible to low-intensity, frequent shaking.

M_{min} has historically been established through expert opinion, which can introduce biases and inconsistencies (Bommer and Crowley 2017). For instance, the definition of M_{min} frequently changes based on the kind of structures being studied and the region's seismicity. M_{min} is normally set at a level where earthquakes below this threshold are considered inconsequential for engineering purposes, as noted by Bommer and Crowley (2017). However, the precise value of M_{min}, especially for low-probability, high-consequence events, can have a substantial impact on the predicted seismic hazard.

A number of research have shown that defining M_{min} requires a more thorough methodology. Bommer and Crowley (2017), for example, stressed how crucial it is to take M_{min} into account in relation to the structural features and the seismic environment. There is not yet a quantifiable, statistically supported approach in the literature for figuring out M_{min}, though. This gap is especially noticeable when considering structural performance, as not enough research has been done on how M_{min} affects the Mean Annual Frequency (MAF) of

various structural limit states. In other words, the literature clearly lacks a systematic investigation, which ought to be quantitative with a statistical basis. In actuality, the definition of M_{min} is unaffected by the earthquake catalogue's lower bound on completeness, the minor magnitude used to fit recurrence relationships, the employed Ground Motion Prediction Equation (GMPE) input variables bounds, etc. (Bommer and Crowley 2017). For a more thorough explanation of these concepts, I refer readers to Bommer and Crowley (2017) who precisely laid out the problem in an engineering context. However, according to Bommer and Crowley (2017), M_{min} is defined as "*M_{min} is the lower limit of integration over earthquake magnitudes such that using a smaller value may result in higher estimate of seismic hazard but would not alter the estimated risk to the exposure under consideration*," which is an engineering explanation of the definition of M_{min} found in the seminal publication by Cornell (1968, p. 1586), which presented the fundamental idea of the PSHA framework and defined M_{min} as: "*… and m_0 is some magnitude small enough, say 4, that events of lesser magnitude may be ignored by engineers*" (m_0 in Cornel's terminology is equivalent to M_{min} in the current terminology). Stated differently, it is not yet proven whether the final risk, commonly defined as the Mean Annual Frequency (MAF) of a given LS (see Azarbakht et al. (2015)), is significantly affected by the high acceleration caused by very close earthquakes with small magnitudes, considering a practical still scientific threshold. Therefore, a systematic, statistically-based method for defining M_{min} is lacking in the literature, and its influence on estimations of seismic hazard and structural performance is still not well understood. In other words, the impact of varying definitions of M_{min} on the Mean Annual Frequency (MAF) of distinct LS has not been adequately examined in previous studies.

Using statistical and probabilistic techniques to identify the cutoff point at which adding earthquakes with lesser magnitudes has no discernible impact on hazard estimations is a more methodical way to define M_{min}. This can be done by determining the point of diminishing returns—the point at which further decreases in M_{min} do not significantly alter the estimated hazard—by examining how sensitive the PSHA results are to various values of M_{min}. It is worth mentioning that the definition of MAF for a certain LS is structure-specific since it is a convolution of hazard and structural performance (Azarbakht et al. 2015). Therefore, it is logical and practical to compute the intended PSHA specifically for a particular structure or structure group. This approach ensures that the seismic hazard assessment is tailored to the unique characteristics and performance requirements of the structure in question, taking into account its specific design parameters, usage, and resilience objectives. By doing so, the results can more accurately reflect the potential risks and inform more effective engineering and safety decisions. Therefore, the MAF saturation strategy, presented in the current manuscript, is one way to tackle this issue. It entails applying several seismic situations to a variety of structural models and doing incremental dynamic analysis. The MAF of various LS as a function of M_{min} can be used to determine the cutoff point, over which adding events of lesser magnitude does not appreciably change the MAF. The ideal value for M_{min} in PSHA can then be determined using this threshold. In this study, we employ structural key factors to accurately depict a wide variety of different structures, with a particular focus on Nuclear Power Plant (NPP) structures. NPP structures were chosen due to their critical importance and the stringent safety requirements they must meet in the face of seismic events. Specifically, we consider both high-frequency, low-ductility structures and low-frequency, variable-ductility secondary systems within NPPs. Therefore a wide variety of structural backbone curves are taken into consideration to comprehensively evaluate the impact of M_{min} on structural performance. The rationale behind this consideration is to capture the range of dynamic responses that

different components of NPPs may exhibit during an earthquake, thus providing a deeper understanding of how M_{min} influences the overall resilience and safety of these essential facilities.

The objective of this research is to fill the highlighted void by methodically investigating the impact of M_{min} on PSHA results and structural safety. In particular, an approach for identifying an ideal M_{min} that strikes a balance between computing efficiency and hazard estimate accuracy will be developed by the present research. By concentrating on several structural kinds, such as low-frequency, variable-ductility secondary systems and high-frequency, low-ductility structures, the study aims to develop recommendations for choosing M_{min} that improve PSHA's dependability for a range of engineering applications.

The current study will use both analytical and empirical methodologies to accomplish these goals. The first step will be a thorough examination of the current M_{min} definitions and how PSHA uses them. An Incremental Dynamic Analysis (IDA) employing a wide variety of SDOF oscillators exposed to diverse earthquake events will come next. The ideal M_{min} is defined as the threshold beyond which lower magnitude events do not appreciably influence the MAF of LS in the context of the MAF saturation technique. Real-world seismic data and structural models will be used to validate the results, guaranteeing the validity and applicability of the suggested methodology.

Besides, a thorough sensitivity analysis must be carried out in order to guarantee the stability of the suggested methodology for defining M_{min}. This entails changing the M_{min} values across a large range and analysing how the PSHA outputs change as a result. Additionally, the influence of various seismic source models, site-specific circumstances, and ground motion prediction equations (GMPEs) should be taken into account in the sensitivity analysis. This will guarantee that the selected M_{min} values are relevant to a broad variety of scenarios and help account for the inherent uncertainties and variability in seismic hazard estimates.

The results show that the predicted ground shaking intensity is strongly affected by the selection of M_{min}, especially for low-probability, high-consequence events and structures with distinctive response features. The suggested methodology can be used for a variety of seismic scenarios and structural types, giving engineers and decision-makers important information for developing and evaluating robust infrastructure.

2 Methodology

Following a three-day workshop, the Electric Power Research Institute (EPRI), in 1989, advocated a constant value of 5 for M_{min} in the NPP industry with the goal of "*establishing a lower-bound earthquake magnitude, below which the potential for damaging to nuclear plants is negligible*". The methods utilised by EPRI (1989) can be summed up as follows: "*The objective of the workshop was to consider a broad range of issues that could provide insight to the engineering significance of ground motion generated by small magnitude earthquakes… it was intended to develop a strategy to select a lower-bound magnitude for use in seismic hazard assessments. An Advisory Committee reviewed the information presented at the workshop and provided recommendations concerning the level of earthquake magnitude that may be damaging to nuclear power plant structures and equipment and a strategy to establish a sound basis to determine the lower bound magnitude*".

As indicated in the IAEA (2010) and other academic articles such as Musson and Sargeant (2007), the M 5 method is a widely accepted value. However, based on the

risk-related definition of M_{min}, this assumption has never statistically been confirmed. Thus, taking into account the structure-specific risk of interest, the present work examines the optimal value for M_{min} for the first time. Thus, by producing a broad range of values for six structural variables—the basic period (T), damping ratio (ξ), and four backbone parameters—a huge range of SDOF oscillators are considered, as seen in Fig. 1. The justification for using SDOF models lies in their simplicity and effectiveness in capturing the fundamental dynamic characteristics of structures. SDOF models are widely used in seismic hazard analysis as well as structural engineering analysis due to their ability to provide clear insights into the primary response modes of structures without the complexity of Multi-Degree of Freedom (MDOF) systems (see Azarbakht and Dolsek 2007, 2011). They are particularly useful in early-stage analyses, where the focus is on understanding the basic principles of structural response to seismic excitations. By employing SDOF models, we can focus on the critical factors influencing structural performance, such as stiffness, damping, and natural frequency, and how these factors interact with seismic inputs of varying magnitudes.

In Fig. 1, LS1 through LS4 stand for, in order, the onset of cracking, the yield point, the beginning of degradation, and the ultimate collapse. As schematically can be seen in Fig. 11 (left), the ratio of the cracking ductility, or D_c/D_y, is the division between the cracking initiation displacement (D_c) and the yielding displacement (D_y); the ultimate ductility, or D_u/D_y, is the ratio between the ultimate displacement (D_u) and the yielding displacement (D_y); the degradation slope, or α_{k0}, denotes the negative slope for the line connecting LS3 to LS4 when the structure degrades to the ultimate failure; and the overstrength factor, or F_c/F_y, is the ratio of the cracking displacement (F_c) and the yielding displacement (F_y). The ten combinations of the overstrength factor and the cracking ductility are displayed in Fig. 1 (right), indicating that this parametric backbone may mimic a broad range of real structural behaviour. This oscillator variant reflects two types of real structures: typical ductile/low-frequency structures like secondary systems that are susceptible to shaking from small-magnitude events, and on the other hand, extremely stiff (high frequency) and low-ductile ones connected to NPP infrastructures. It is important to note that the SDOF oscillators are currently described by six parameters. Later in this work, we shall examine

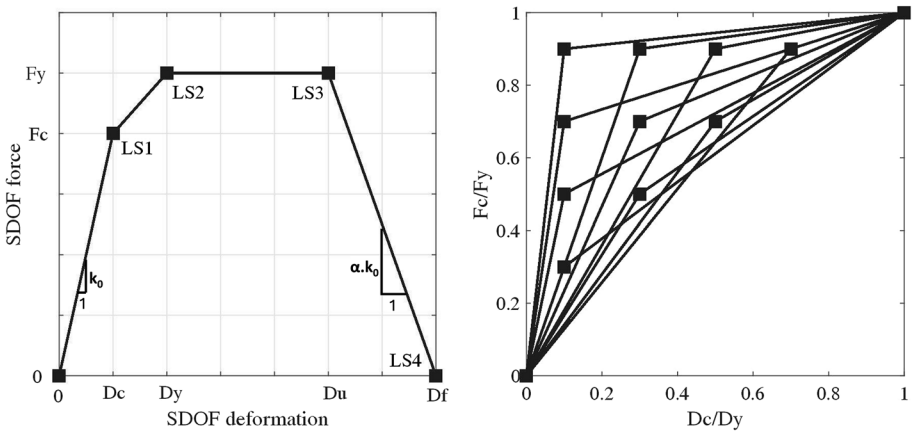

Fig. 1 (left) Definition of the backbone curve with controlling parameters and LS1 to LS4; (right) all different possible combinations of the backbone curves for the ratios F_c/F_y and D_c/D_y between 0 and 1 (also see Azarbakht and Amini 2018)

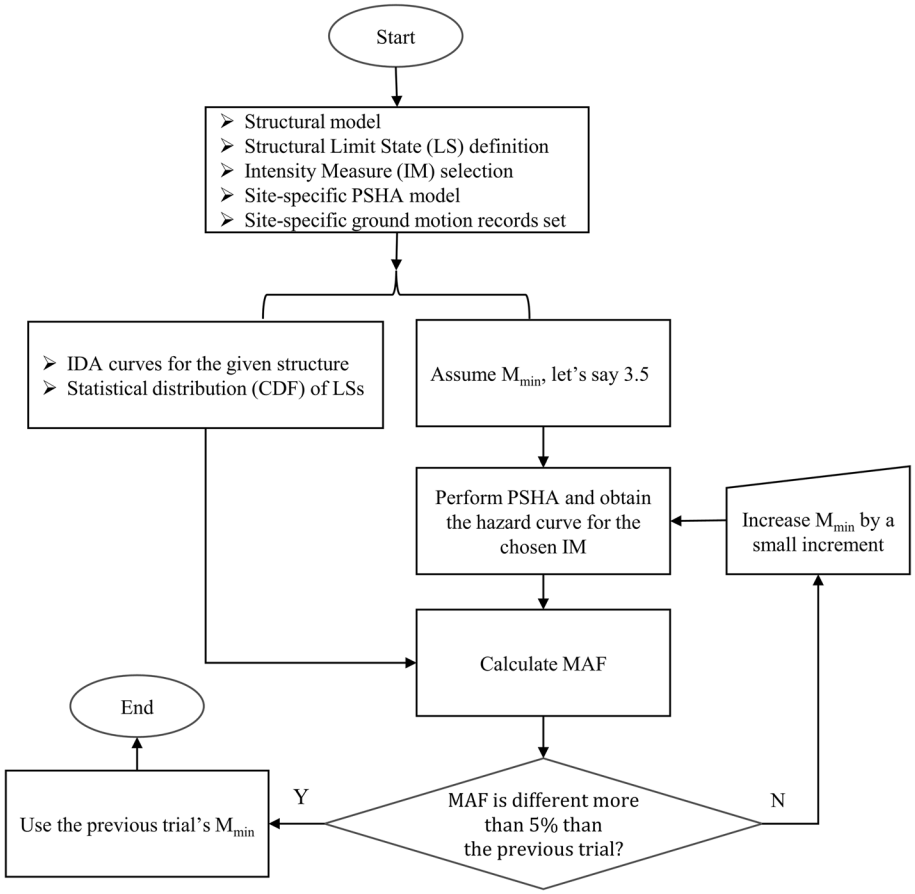

Fig. 2 Flowchart demonstrating the process of determining the ideal M_{min} using the MAF saturation strategy presented in this study

the additional six variables that reflect the hazard circumstances which are introduced in Sect. 4.

The current study introduces the "MAF saturation strategy" methodology for the first time. It searches for the cut-off magnitude at which the MAF remains constant (taking into account a workable yet scientific threshold) if lower values of this cut-off are employed as M_{min} for the hazard estimates. In order to derive the corresponding LS (including the collapse capacity defined as the global structural instability) points for each oscillator case, an Incremental Dynamic Analysis (IDA) (Vamvatsikos and Cornell (2002)) is carried out using the Hunt and Fill algorithm for a set of chosen ground motions [see also Azarbakht and Dolsek (2007, 2011)]. To capture the variety in structural response, the IDA requires exposing the structure to a set of ground motion records, each scaled to several intensity levels. The Hunt and Fill algorithm is used for this, first doubling/tripling the intensity measure in each trial to capture the collapse capacity point with the least trials. The capacity point in an IDA curve is the final non-infinity point in an IDA curve. A predetermined number of IDA points—20 total in this study—are computed to bridge the gap between

the origin and the capacity point while the capacity point is being pursued. This algorithm was selected due to its effectiveness in striking a balance between computational effort and efficiency. Peak Ground Acceleration (PGA) as an IM is used for each individual nonlinear response-history analysis. As will be covered in Sect. 3, the IDA curves are eventually converted to the spectral acceleration IM. Thus, the distribution of LS versus Intensity Measure (IM) is obtained, and the structure-specific MAF can be determined by convolving with the hazard curve [for further information, see Gkimprixis et al. (2019) and Azarbakht et al. (2015)]. To get the cut-off lower magnitude (M_{min}), repeat this convolution for a range of M_{min} values while acknowledging a reasonable engineering threshold that is still scientific. When lower values are utilised as M_{min} in the PSHA computation, this cut-off is defined as the MAF's value does not vary much (with a modest supplied threshold). Consequently, the minimum magnitude limit that needs to be considered in a comprehensive PSHA investigation is the obtained optimum M_{min} as is discussed in the following sections. The process of calculating the optimum M_{min} based on the MAF saturation strategy for a particular structure in a given site is illustrated in Fig. 2.

3 IDA and numerical fragility functions for a given set of SDOF oscillators

A common method for estimating structural seismic demand and capacity is response history analysis (Katsanos et al. 2010). For the aim of performance-based earthquake engineering, IDA is the most often used algorithm for numerically determining the nonlinear response of structures (Vamvatsikos and Cornell 2002). IDA uses a detailed model of a particular structure and, as a result, evaluates the nonlinear response history for a collection of ground motion records that are scaled to several degrees of seismic motions, ranging from elastic behaviour to global instability (Vamvatsikos and Cornell 2002). The most popular IMs are Sa(T1,5%), Spectral Acceleration at the natural period of a certain structure (T1) and 5 per cent damping ratio, PGA, Peak Ground Velocity (PGV), and so on (see also Baker (2005); Mehanny (2009); Tothong and Luco (2007); Ebrahimian et al. (2015); O'Reilly (2021). The relationship between the annual rate of exceedance (seismic hazard) and the structural response is significantly influenced by IM (see Vargas-Alzate et al. 2022; Ghafory-Ashtiany et al. 2011 and 2012; Mousavi et al. 2011). The literature contains a number of IMs, each with potential drawbacks and some form of gain (Luco and Cornell 2007). However, because $S_a(T_1, 5\%)$ is the most widely used and practical IM in the literature currently accessible, it has been used throughout the current study. We acknowledge that using other IMs is a topic worth investigating further, but we also believe this topic is outside the purview of the current study.

In order to mimic the seismic response of reinforced concrete buildings, this work focused on NPP infrastructures and created a seismic response database for the SDOF oscillators. NPPs were chosen as the reference for modelling the behaviour of RC structures due to their critical importance and stringent safety requirements, which necessitate a thorough understanding of seismic performance. NPP structures often embody high-frequency, low-ductility characteristics, as well as low-frequency, variable-ductility secondary systems, providing a comprehensive representation of different structural responses under seismic loading. Although alternative options, such as standard residential or commercial RC buildings, were considered, NPPs were ultimately selected because their failure consequences are significantly higher, and thus their study provides more rigorous insights

into the resilience and reliability of RC structures under extreme seismic events. This focus ensures that the findings are applicable to a wide range of critical infrastructure, contributing to broader safety and engineering standards. To achieve this, a piecewise four-linear backbone curve was created, as shown in Fig. 1, to resemble the static pushover curve of the corresponding SDOF system as well as the MDOF. A typical four-linear backbone curve, as shown in Fig. 1 (left), starts elastically up to the cracking point (LS1), yields at $D_c/D_y = 1$ (LS2), is fully plastic up to D_u, and then begins to degrade with a slope α_{k0} (where k_0 is the elastic slope) until the zero strength. This curve represents a wide range of conventional NPP structures. It is important to note that the considered backbone curve's shape is determined by four primary parameters: α, D_c/D_y, D_u/D_y, and F_{cr}/F_y. Almost any pushover curve can be fitted with the idealised curve by appropriately varying these four parameters. However, pushover curves exhibiting highly irregular or non-standard behaviour due to complex interactions or highly unique structural characteristics may not fit as accurately with the idealised curve. These exceptions typically arise in cases where structural irregularities, non-uniform material properties, or unconventional load distributions significantly deviate from the assumptions underlying the idealised model. Therefore, while the idealised curve is broadly applicable, it is important to recognise its limitations in capturing the full range of possible structural behaviours.

The period (T) and damping ratio (ξ), the latter of which is presumed to be mass proportionate, are additional structural input factors. Assumed to be constant and equal to 0.5, the β parameter characterises the unloading stiffness of Takeda's hysteretic rules (Takeda et al. 1970). The nonlinear hysteretic behaviour of the structures was captured using the Takeda uniaxial material model, which accurately represents stiffness degradation, strength deterioration, and pinching effects under cyclic loading. A displacement-based approach was employed for the nonlinear analysis, utilising the Newton–Raphson iterative method and, when necessary, alternative algorithms like Modified Newton and NewtonLineSearch to ensure robust convergence. The structural model included an inverse pendulum consisting of mass, elastic stiffness, critical damping ratio and the nonlinear backbone curve modelled by one-component lumped plasticity element. Geometric nonlinearities were considered through appropriate transformations to capture large displacements. Rayleigh damping was implemented with specified coefficients for mass to model energy dissipation. Time integration was performed using the Newmark-beta method, ensuring numerical stability and accuracy (Mazzoni et al. 2006).

To elaborate, the SDOF-IDA curves were computed for eleven different values of the period (T = 0.1, 0.2, 0.3, 0.4, 0.5, 0.75, 1, 1.25, 1.5, 1.75, and 2.0 s), for two different degradation slopes (α = − 0.05 and − 0.5), ten different combinations of F_c/F_y and D_c/D_y (refer to Fig. 1 (right)), for seven different values of the ultimate ductility (D_u/D_y) (2, 3, 4, 5, 6, 7, and 8) and three damping ratios (1, 3 and 5%). For every chosen ground motion record, 4620 SDOF-IDA curves must be calculated using all possible permutations of the stated structural input parameter of the SDOF system. The OpenSees platform was used for all nonlinear dynamic analyses (Mazzoni et al. 2006).

The effects of moderate-low magnitude near-earthquake events on PSHA findings have not been extensively discussed in the existing literature. However, these events can significantly influence seismic hazard assessments, particularly in regions with high seismicity. Moderate-low magnitude earthquakes, while not as catastrophic as large-magnitude events, can occur more frequently and thus contribute to the cumulative seismic risk. They may cause considerable damage, especially to structures not designed to withstand frequent seismic activities. For example, Bommer and Abrahamson (2006) discuss the implications of near-field ground motions, noting that even moderate-magnitude earthquakes can

produce high-frequency shaking capable of damaging structures. Moreover, recent studies such as Rodriguez-Marek et al. (2013) highlight the importance of including moderate earthquakes in PSHA models to ensure a more comprehensive risk assessment. Ignoring these events could lead to an underestimation of seismic hazard, particularly in areas where such earthquakes are common. Therefore, our study acknowledges and incorporates the influence of moderate-low magnitude earthquakes to provide a more accurate and realistic representation of seismic risk. Therefore, we have selected a collection of near-filed ground motion records for SDOF analysis. As a result, 31 near-source (closest source-to-site distance, R_{close}, less than 16 km) strike-normal ground motion components that were captured from four distinct earthquakes under forward directivity circumstances are taken into consideration. Each ground motion was uniformly processed for the PEER Strong Ground Motion Database after being captured on NEHRP (BSSC 1994) S_D or S_C site classifications (Chiou et al. 2008). Sc site classification refers to an average shear-wave velocity to depth of 30 m between 360 and 760 m/s while this range is between 180 and 360 m/s in the S_D case. Table 1 provides a summary of the record attributes, while Fig. 3 displays the 5% damped elastic response spectrum.

It is worth noting that the ground motion records used in this study have a near-fault effect at distances less than 16 km. Near-fault ground motions are characterised by distinct features such as forward directivity and fling step, which can significantly impact the seismic response of structures (Somerville et al. 1997; Mavroeidis and Papageorgiou 2003). These features result in strong, long-period pulses in the velocity time histories, which can lead to higher demands on structures compared to far-field ground motions. In the context of this study, the inclusion of near-fault ground motion records is particularly relevant for assessing the seismic performance of SDOF oscillators. The proximity to the fault and the associated directivity effects can amplify the response, necessitating a thorough evaluation of these records to ensure an accurate representation of the seismic hazard for small magnitudes with high amplitudes. The impact of near-fault effects on the results of this study is twofold. Firstly, the increased amplitude and energy content in the near-fault records can lead to higher displacement demands on the SDOF oscillators, thereby influencing the derived fragility functions. Secondly, the variability and intensity of these records contribute to the overall uncertainty in the seismic response, highlighting the need for robust modelling approaches to account for these effects. By including near-fault ground motions, the study provides a more comprehensive assessment of the seismic risk, particularly for infrastructures located in close proximity to active faults.

Using the Hunt and Fill tracing algorithm, the IDA analyses are carried out for all selected SDOF oscillators for each of the ground motion records in Table 1 (Vamvatsikos and Cornell 2002). Each of the twenty distinct points on an IDA curve is derived from a nonlinear response history study of a specific SDOF oscillator (refer to Fig. 1). As can be seen in Fig. 4 for a specific SDOF oscillator example, the IDA curves are first calculated for the PGA, which is an IM. From there, they can be easily linearly transformed to any further new linear IMs, such as the spectral acceleration at the period of the SDOF system with a 5% damping ratio, $S_a(T_1, 5\%)$.

The Cumulative Distribution Function (CDF) of IMs in a given Engineering Demand Parameter (EDP) for a specific LS is derived using a set of 31 IDA curves for a given SDOF oscillator (see Fig. 1). In this study, the ductility demand (the division of nonlinear displacement response over yielding displacement, D_y) is simply called EDP. For instance, Fig. 5 displays the IM empirical CDF distributions vs $Sa(T_1, 5\%)$, corresponding to LS1 to LS4. For example, every LS in Fig. 1 is associated with an EDP value. Hence, all the IDA curved are interpolated to that given EDP, and 31 corresponding $Sa(T_1, 5\%)$ values

Table 1 Near-field earthquake ground motion records

Earthquake Location	Year	M_w	Station	R_{close} (km)	PGA (%g)
(1) Imperial Valley	1979	6.5	Brawley Airport	8.5	0.158
(2)	Same as above		EC County Center FF	7.6	0.180
(3)			EC Meloland Overpass FF	0.5	0.378
(4)			El Centro Array #1	15.5	0.138
(5)			El Centro Array #4	4.2	0.357
(6)			El Centro Array #5	1.0	0.375
(7)			El Centro Array #6	1.0	0.442
(8)			El Centro Array #7	0.6	0.462
(9)			El Centro Array #8	3.8	0.468
(10)			El Centro Array #10	8.6	0.176
(11)			El Centro Array #11	12.6	0.370
(12)			El Centro Differential Array	5.3	0.417
(13)			Westmorland Fire Sta	15.1	0.077
(14)			Parachute Test Site	14.2	0.135
(15) Superstition Hills (B)	1987	6.7	El Centro Imp. Co. Cent	13.9	0.308
(16)	Same as above		Westmorland Fire Sta	13.3	0.210
(17)			Parachute Test site	0.7	0.419
(18) Loma Prieta	1989	6.9	Saratoga—W Valley Coll	13.7	0.403
(19) Northridge	1994	6.7	Canyon Country—W Lost Cany	13.0	0.466
(20)	Same as above		Jensen Filter Plant #	6.2	0.393
(21)			Newhall -Fire Sta #	7.1	0.724
(22)			Rinaldi Receiving Sta #	7.1	0.887
(23)			Sepulveda VA #	8.9	0.722
(24)			Sun Valley—Roscoe Blvd	12.3	0.298
(25)			Sylmar—Converter Sta #	6.2	0.594
(26)			Sylmar—Converter Sta East #	6.1	0.839
(27)			Sylmar—Olive View Med FF #	6.4	0.733
(28)			Arleta—Nordhoff Fire Sta #	9.2	0.237
(29)			Newhall—W. Pico Canyon Rd	7.1	0.426
(30)			Pacoima Dam (downstr) #	8.0	0.499
(31)			Pacoima Kagel Canyon #	8.2	0.527

are obtained. These 31 $Sa(T_1, 5\%)$ values have a statistical distribution i.e. empirical cumulative distribution function as shown in Fig. 5. Given that the given SDOF behaviour is substantially more nonlinear at LS3 and LS4 than it is at LS1 and LS2, the LS1 and LS2 empirical CDF distributions exhibit significantly less dispersion when compared to the LS3 and LS4 CDF distributions. Stated otherwise, since SDOF behaviour is linear and any ground motion record has the same structural response, the dispersion at LS1 is theoretically zero (this is not the case when an MDOF structure is picked for further investigation). It is still in the early stages of nonlinear behaviour at LS2, and substantial levels of nonlinearity are anticipated in LS3 and LS4. It is also important to note that in order to compute

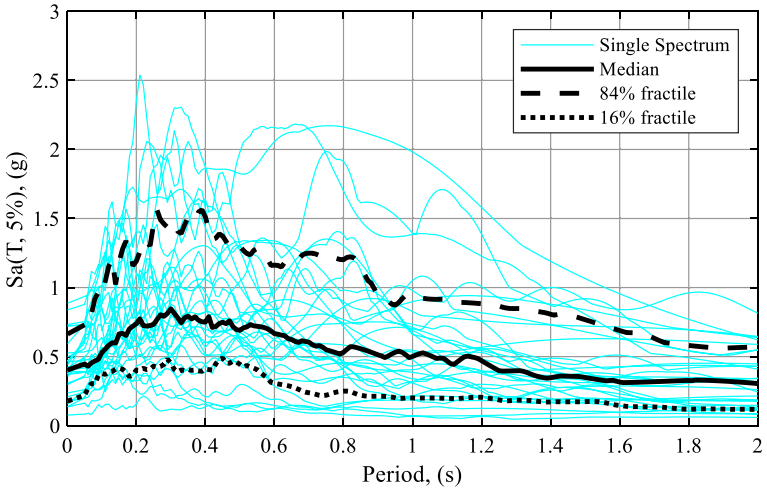

Fig. 3 The 5 per cent damped elastic response spectra for the 31 selected records

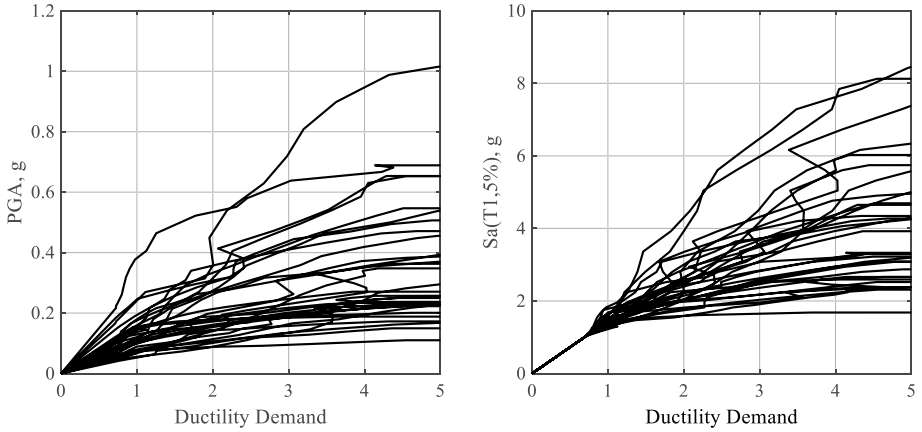

Fig. 4 (Left) The IDA curves versus PGA for an SDOF system with T = 1 (s), damping ratio = 5 per cent, $D_c/D_y = 0.7$, $D_u/D_y = 4$, $F_c/F_y = 0.9$ and $\alpha = -0.5$; (right) the same IDA curves in (left) versus $S_a(T_1, 5\%)$

MAF for a specific structure, the resulting empirical CDF distributions will be convoluted with the hazard function in the following sections. After that, we can compare the MAF discrepancy to the M_{min} to make more inferences.

4 PSHA calculation for a point seismic source model

We must choose from a large variety of constructions and take into account a fictitious seismicity scenario. To achieve this, we begin with a basic illustration of a traditional seismic point source. Further research, however, may include a more complex seismicity model, such

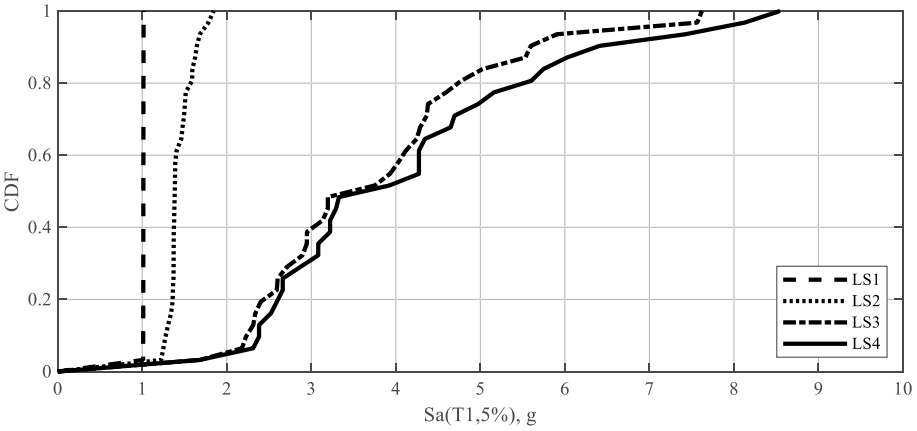

Fig. 5 The empirical CDFs corresponding to different LSs are defined in Fig. 1 and the SDOF oscillator is defined in Fig. 4

as one that incorporates a linear source, an area source, or an actual location with multiple intricate seismic sources. Six variables are required to define this simple point source seismicity: the Gutenberg and Richter (1955) constants, a=4.5 and b=1, the minimum and maximum moment magnitudes, M_{min} and M_{max}=7.5, the (Joyner-Boore) distance, R_{jb}, from the point source to the given site, and a given GMPE (see McGuire 1995, 2007 and Baker et al. 2021). Because of its great stability, the Chiou and Youngs (2014) GMPE is used in the present work (Bommer and Stafford 2020).

Uncertainty in the hazard model arises from several sources, including the variability in the Gutenberg-Richter parameters (a and b), the minimum and maximum magnitudes (M_{min} and M_{max}), the distance to the point source (R), and the chosen GMPE. While this study incorporates reasonable deterministic assumptions for these variables, the only available source of uncertainty is the given GMPE. However, we have only used the GMPE median values in this study. Therefore, future work could explore the impact of these uncertainties more rigorously. For instance, variations in the a and b values can significantly alter the predicted seismicity rates, and different GMPEs can yield different hazard estimates. Additionally, uncertainties in site-specific parameters like V_{s30} and Z_{10} (defined in the next paragraph) also contribute to the overall uncertainty in the hazard model. Recognising and quantifying these uncertainties is crucial for a comprehensive PSHA.

It is important to note that for the sake of this study, the depth (D) is taken to be equivalent to 10 km. Consequently, one can compute the rupture distance (R_{rup}) using the formula $\sqrt{{R_{jb}}^2 + D^2}$. The depth (D) and the depth to the top of the rupture, Z_{TOR}, are the same. It is assumed that the shear wave velocity (V_{s30}) averaged over the above 30 m in m/s represents a bedrock of 1200 m/s. Z_{10}, the basin depth, is computed in relation to V_{s30} (Chiou and Youngs 2014). A strike-slip fault mechanism is represented by the fault dip angle (δ) of 0.9 and the rake angle (λ) of zero in degrees. The PSHA in its most general form can be written as Eq. (1).

$$\lambda(y) = \nu \iint f_M(m) f_R(r) P[Y > y|m, r] dmdr \tag{1}$$

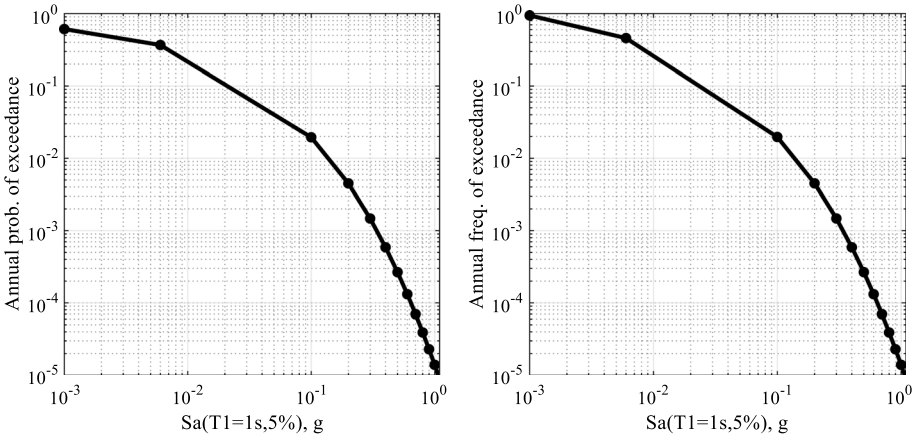

Fig. 6 The annual probability of exceedance (left) and the annual frequency of exceedance for a point source 10 km away from a given fictitious site of study

where $f_M(m)$ and $f_R(r)$ are the probability density functions associated with magnitude (M) and distance (R), respectively. $\lambda(y)$ is the rate of occurrence of ground motions with an IM > y. P[Y > y| m,r] is obtained using a suitable GMPE. For a given seismic source, ν is the rate of occurrence of earthquakes larger than a M_{min} ($\nu = 10^{(a-bM_{min})}$).

In this study, the six seismicity variables are, strictly speaking, a, b, M_{min}, M_{max}, R, and GMPE. We have made some reasonable assumptions for these six factors for the time being. For instance, Fig. 6 displays the outcome of the PSHA analysis for a point source located 10 kms distant from a fictitious site of interest, using the previously stated set of input parameters. Figure 6 (left) displays the annual probability of exceedance (assumed to be a Poisson distribution) versus IM, while Fig. 6 (right) displays the annual frequency of exceedance. To meet the practical needs of engineering, the horizontal axis, which represents the IM range, is displayed between 0.001 g and 1 g. To calculate MAF, however, a larger range of IM has been used in order to encompass the whole numerical extent of interest.

5 M_{MIN} based on the proposed MAF saturation strategy

The estimation of the median threshold and the widely accepted log-normal distribution (or, in reality, any other suitable distribution) can be used to build a fragility function, with a certain standard deviation indicating the degree of uncertainty in damage initiation. Nonetheless, as mentioned in Sect. 3, we have applied the experimental fragility curves based on IDA curves in the current investigation. Thus, the MAF of exceedance of a certain LS can be used to illustrate the risk associated with a given structure. The CDF for the fragility curve is represented by P in the following (see Fig. 5), and the probability of a given LS at a particular IM is indicated by P(LS| im) (see Fig. 6-left). As a result, we can use Eq. (2) to calculate the MAF value of an LS (λ_{LS}) [also see Azarbakht et al. (2015)].

$$\lambda_{LS} = \int_0^{\infty} P(\text{LS}|\ \text{im}) \left| d\lambda_{IM}(im) \right| \tag{2}$$

where the hazard curve acquired via PSHA is represented by $\lambda_{IM}(im)$, and the symbol d stands for the differentiation operator. It appears that the occurrence of earthquakes with varying strengths may be the cause of the LS exceedance event (Cornell 2005). In other words, when a single SDOF oscillator approaches a specific LS (LS1 to LS4 in Fig. 1), the Sa(T_1, 5%) can change for various ground motions in Table 1. For instance, in PSHA computations, the MAF values are computed in relation to various M_{min} values; the outcomes are displayed in Fig. 7 with respect to varying site-to-source distance. It was predictable that when the site-to-source distance increases, the MAF value will decrease, as seen in Fig. 7. On the other hand, as the site-to-source distance grows, the dispersion in MAF values also decreases too. Put another way, the degree of dispersion increases with

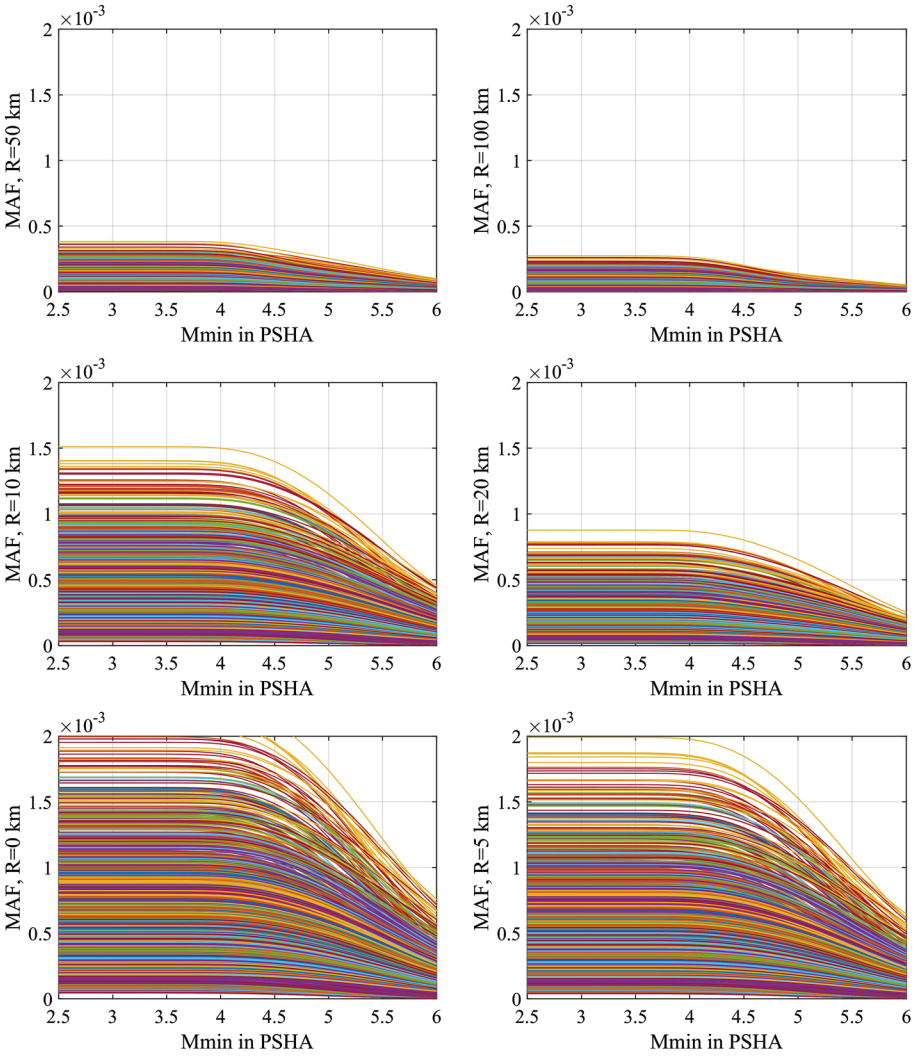

Fig. 7 The MAF versus the variation of M_{min} in PSHA calculation and for different site-to-source distances. 4620 curves are plotted for all the considered SDOF oscillators

our proximity to the spot. This demonstrates why choosing M_{min} in near-field hazard investigations is far more crucial. Despite the site-to-source distance, as shown in Fig. 7, the ideal M_{min} value seems to be closer to 4 rather than the conventional value of 5. Figure 7 shows that, when M_{min} is taken to be equal to 4 and 5, there is a significant variation in the calculated MAF values, intuitively almost as a factor of 2–3. The results also show that the MAF is less structure-specific when the potential seismic source has a farther distance (e.g. 100 km) when compared to the nearer distance (e.g. 0 or 5 km). This shows that MAF is highly structure-specific in near-field seismic sources and gets less structure-specific when the seismic sources get farther.

6 Discussion on the obtained results

Figure 7 illustrates how, although at varying amplitudes, the MAF value for every SDOF oscillator essentially follows the same form. As stated otherwise, the curves begin to decline beyond the magnitude equal to 4, while the MAF value is intuitively constant before then. The ideal M_{min} values, based on the MAF saturation technique, are displayed versus six structural characteristics as seen in Fig. 8. According to intuition, the natural period of a certain structure is the single factor that determines the optimal M_{min} (Fig. 8 bottom-left). For high-frequency structures, the ideal M_{min} ranges below 4.2, while for low-frequency structures, it increases to 4.3. However, the widely accepted assumption of 5 is not supported in this instance and should be modified in the literature that is currently accessible, particularly when the seismic hazard is intended to be applied to low-period structures, such as NPPs.

In addition, as Fig. 9 illustrates, the relationship between the MAF value at R = 0 km and the MAF value at R = 100 km is tracked against the other six structural factors in order to provide more context for this phenomenon. As Fig. 9 (bottom-left) illustrates intuitively, the crucial parameter in this behaviour is the natural period of the SDOF oscillator. Furthermore, for a given T in Fig. 9 (bottom-left), there is very little variation in the responses of the various oscillators. Put differently, about the same MAF ratio is produced by many oscillators with the same T value. We infer that the primary control factor for both the MAF itself and the M_{min} optimal value is the oscillator's natural period of vibration. For this reason, we suggest using Eq. (3) to determine M_{min} in PSHA research, with the structural period of interest being the basis for this calculation.

$$M\_min = \begin{cases} 4 & T \leq 0.1 \\ 4.1 & 0.1 < T \leq 0.4 \\ 4.1 & 0.4 < T \leq 0.5 \\ 4.3 & 0.5 < T \end{cases} \tag{3}$$

We tested an oscillator, the same as the oscillator in Fig. 4, under two different conditions: first, by implementing M = 4 as the optimum value, and second, by implementing M = 5 as an arbitrary (or, more accurately, based on the common choice in the literature) value. This allowed us to better understand the significance of the optimum M_{min} values. The hazard curves are computed for four situations, as shown in Fig. 10 (top-left), where R = 0 km in combinations with M = 4 and 5, and R = 100 km in combinations

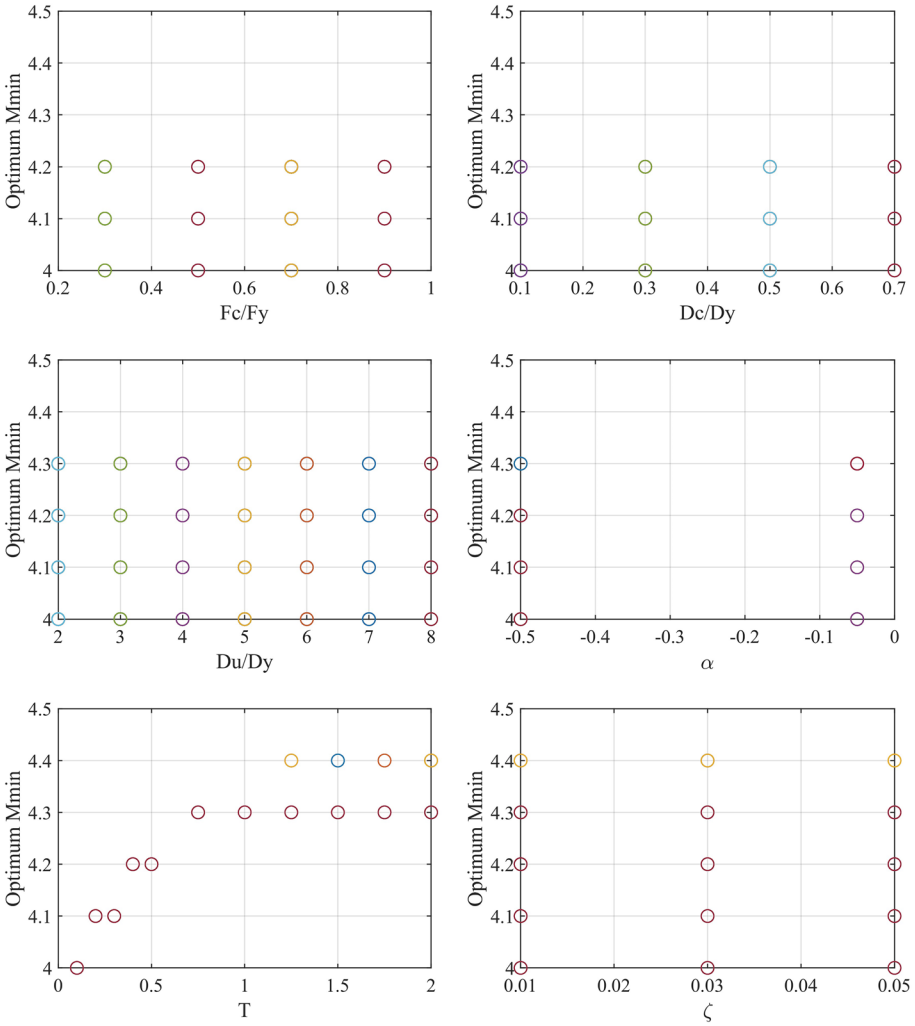

Fig. 8 The optimum M_{min} values, based on the MAF saturation strategy, and versus six structural parameters. Each subplot for 4620 SDOF oscillators shows 4620 points with various colours, some of which are identical

with M = 4 and 5. This figure illustrates how, depending on the two M_{min} that are used, each hazard curve splits into two branches when it reaches the low IM values. To accurately reflect this difference, we have employed refined IM intervals in this area. The fragility curve for the specified SDOF oscillator (as in Fig. 4) corresponding to LS4 is shown in Fig. 10 (top-right). In the case of R = 0 km and R = 100 km, the MAF fluctuations versus Sa(T1, 5%) are displayed in the bottom-left and bottom-right figures, respectively. The MAF for this structure varies depending on whether the M_{min} value is 4 or 5, as can be shown in Fig. 10 bottom-left and bottom-right. The MAF values are listed at the top of each figure in each case; however, we have defined the error as given in Eq. (4) in order to more clearly show the error extent.

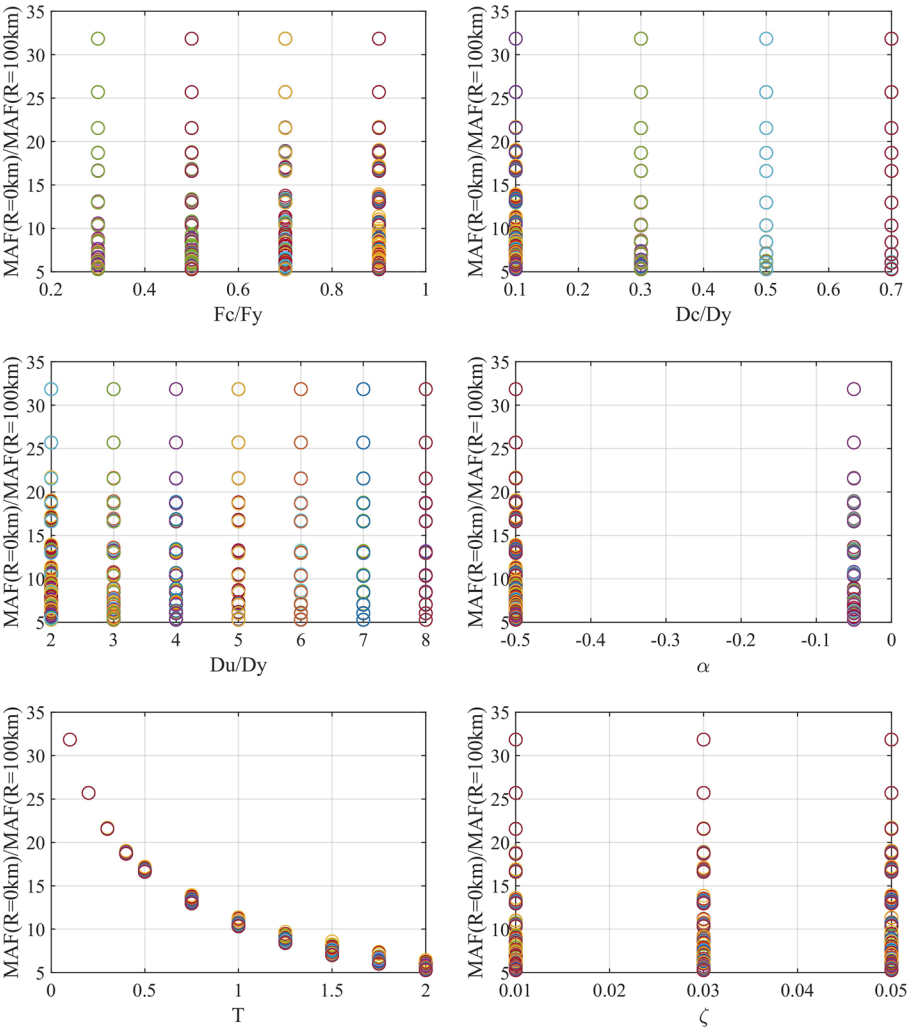

Fig. 9 The ratio of MAF with a hazard at R = 0 km divided by the MAF with a hazard at R = 100 km versus the different six structural parameters. Each subplot for 4620 SDOF oscillators shows 4620 points with various colours, some of which are identical

$$Error = 100 \times \left| \frac{MAF(M=5) - MAF(M=4)}{MAF(M=5)} \right| \tag{4}$$

Figure 11 displays the computed inaccuracy against the SDOF oscillator natural period of vibration and for various site-to-source distances. As seen in Fig. 11, this inaccuracy, which ranges from 20 to 120 per cent and is mostly a function of the natural period. The inaccuracy decreases with increasing T in the near-field, which is defined as the site-to-source distance of less than 20 km. For longer distances, the inaccuracy grows with increasing the natural period until a certain point, approximately T = 0.75 s. Future research will focus on this tendency, which is primarily dependent on the used GMPE.

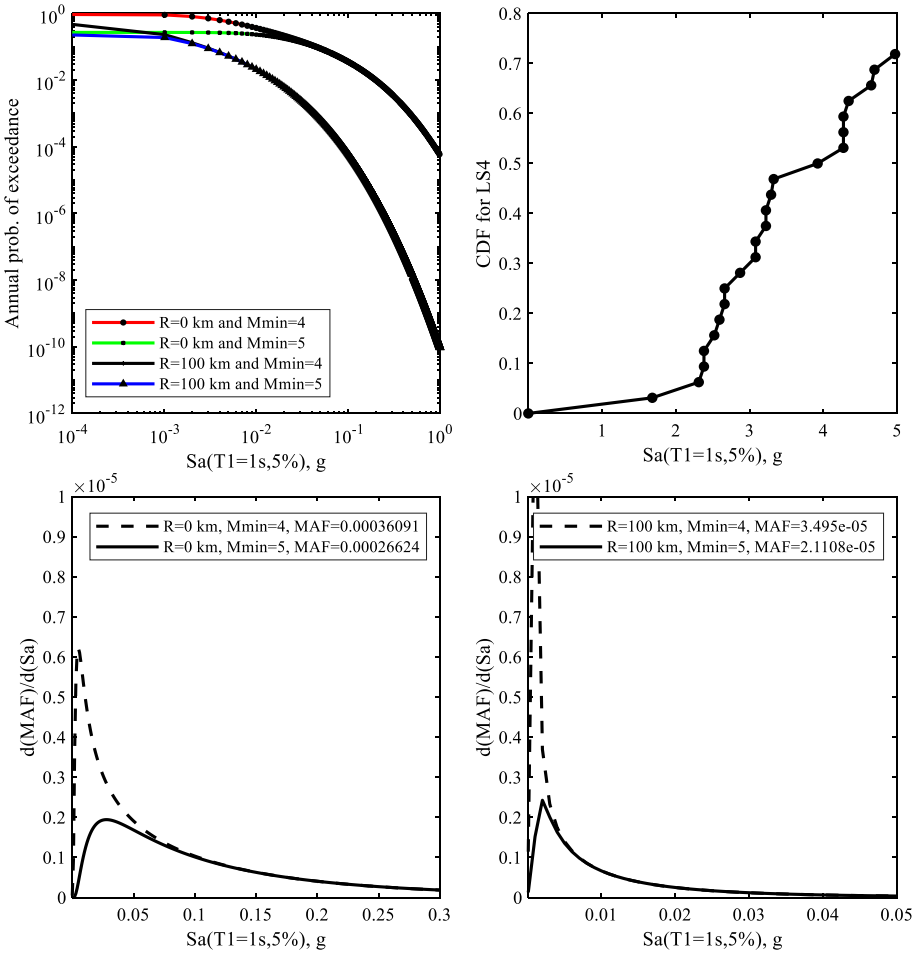

Fig. 10 (Top-left): The hazard curves for R = 0 and 100 km for tow M_{min} values of 4 and 5; (top-right): the fragility curve corresponding to the LS4 and for the SDOF oscillator in Fig. 3; (bottom-left): MAF versus Sa(T1, 5%) in the case of R = 0 km; (bottom-right): MAF versus Sa(T1, 5%) in the case of R = 100 k

7 Conclusions

The PSHA computation takes a wide range of M_{min} into account to investigate how they affect the MAF values for a variety of SDOF structures. To this end, 31 near-field ground motion records and the structure response in all possible IM ranges have been recorded using IDA. Structure-specific MAF values are then determined by quantitatively deriving the fragility curve for a certain LS from IDA curves and combining it with hazard cures. The findings showed that in order to precisely capture the MAF of interest, the M_{min} value between 4 and 4.3 must be taken into consideration. Put differently, there could be a substantial difference in the MAF values (up to around 120 per cent inaccuracy) if a value of 5 is used in the PSHA computation. This finding contradicts the commonly accepted $M_{min} = 5$ for NPP infrastructures. Furthermore, it is demonstrated that the optimal M_{min} value is a direct function of the natural period of the oscillator rather than a significant

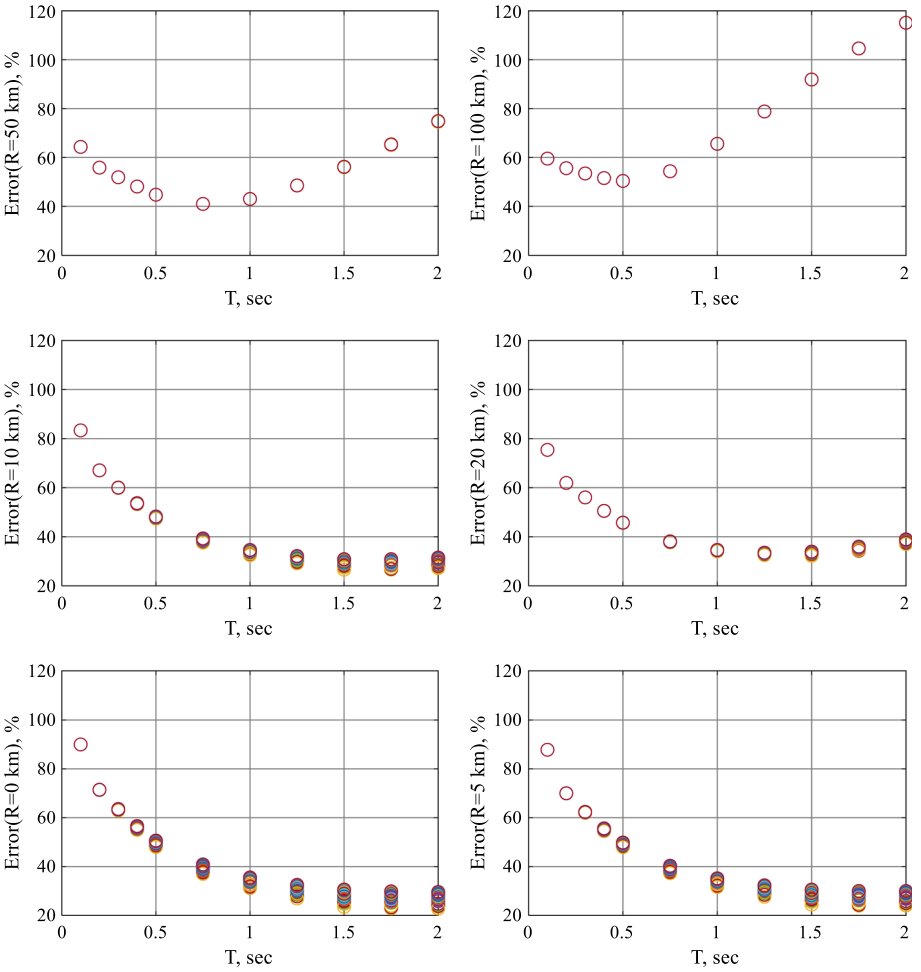

Fig. 11 The error value, based on Eq. (4), versus the natural period of oscillation and for different site-to source distance

function of the other structural features. In general, smaller M_{min} values must be taken into account for the stiffer structures. Additionally, utilising bigger M_{min} numbers (instead of the ideal/optimum M_{min} value) introduces a level of error depending on the natural period of the structure. It is important to note that all of the conclusions were derived using presumptions from this study and should not be automatically generalised to other scenarios. In particular, it is necessary to look into the impact of additional seismic conditions, such as a genuine site with multiple seismic faults. Another area that needs attention is the uncertainty in the various PSHA aspects. The focus of the current study is on SDOF oscillators; however, MDOF structures with a large contribution from higher modes are still accessible for exploration.

Acknowledgements We thank both anonymous reviewers for their invaluable comments on a previous version of this study which substantially improved the paper.

Funding This study was not supported by any funding resources.

Data availability The ground motion records are based on the PEER database. Any further reasonable data request can be make via an email to the author.

Declarations

Conflict of interest The author has no relevant financial or non-financial interests to disclose.

References

Azarbakht A, Amini S (2018) Statistical distribution of intensity measures to obtain input for incremental dynamic analysis. In: 16th European conference on earthquake engineering, Thessaloniki

Azarbakht A, Shahri M, Mousavi M (2015) Reliable estimation of the mean annual frequency of collapse by considering ground motion spectral shape effects. Bull Earthq Eng 13(3):777–797

Azarbakht A, Dolšek M (2011) Progressive incremental dynamic analysis for first-mode dominated structures. J Struct Eng 137(3):445–455

Azarbakht A, Dolšek M (2007) Prediction of the median IDA curve by employing a limited number of ground motion records. Earthq Eng Struct Dyn 36(15):2401–2421

Baker JW, Bradley BA, Stafford PJ (2021) Seismic hazard and risk analysis. Cambridge University Press, Cambridge

Baker J.W. (2005). Vector-valued ground motion intensity measures for probabilistic seismic demand analysis, *Stanford University*.

Bommer JJ, Stafford PJ (2020) Selecting ground-motion models for site-specific PSHA: adaptability versus applicability. Bull Seismol Soc Am 110(6):2801–2815

Bommer JJ, Crowley H (2017) The purpose and definition of the minimum magnitude limit in PSHA calculations. Seismol Res Lett 88(4):1097–1106

Bommer JJ, Abrahamson NA (2006) Why do modern probabilistic seismic-hazard analyses often lead to increased hazard estimates? Bull Seismol Soc Am 96(6):1967–1977

BSSC (1994) NEHRP recommended provisions for seismic regulations for new buildings, Part 1—Provisions. FEMA 222A, Federal Emergency Management Agency.

Chiou BSJ, Youngs RR (2014) Update of the Chiou and Youngs NGA model for the average horizontal component of peak ground motion and response spectra. Earthq Spectra 30(3):1117–1153

Chiou B, Darragh R, Gregor N, Silva W (2008) NGA project strong-motion database. Earthq Spectra 24(1):23–44

Cornell CA (2005) On earthquake record selection for nonlinear dynamic analysis. In: Proceeding of the Luis Esteva symposium, Mexico

Cornell CA (1968) Engineering seismic risk analysis. Bull Seismol Soc Am 58(5):1583–1606

Ebrahimian H, Jalayer F, Lucchini A, Mollaioli F, Manfredi G (2015) Preliminary ranking of alternative scalar and vector intensity measures of ground shaking. Bull Earthq Eng 13:2805–2840

EPRI (1989) Engineering characterisation of small-magnitude earthquakes. EPRI Report NP-6389, Electric Power Research Institute, Palo Alto, California

Ghafory-Ashtiany M, Mousavi M, Azarbakht A (2011) Strong ground motion record selection for the reliable prediction of the mean seismic collapse capacity of a structure group. Earthq Eng Struct Dyn 40(6):691–708

Gkimprixis A, Tubaldi E, Douglas J (2019) Comparison of methods to develop risk-targeted seismic design maps. Bull Earthq Eng 17(7):3727–3752

Gerstenberger MC, Marzocchi W, Allen T, Pagani M, Adams J, Danciu L, Petersen MD (2020) Probabilistic seismic hazard analysis at regional and national scales: state of the art and future challenges. Rev Geophys. https://doi.org/10.1029/2019RG000653

Gutenberg B, Richter CF (1955) Magnitude and energy of earthquakes. Nature 176(4486):795–795

IAEA (2010) Seismic hazard in site evaluation for nuclear installations. Specific Safety Guide No. SSG-9, International Atomic Energy Agency, Vienna, Austria, p 80

Katsanos EI, Sextos AG, Manolis GD (2010) Selection of earthquake ground motion records: a state-of-the-art review from a structural engineering perspective. Soil Dyn Earthq Eng 30(4):157–169

Kramer SL (1996) Geotechnical earthquake engineering. Prentice Hall, Upper Saddle River

Luco N, Cornell CA (2007) Structure-specific scalar intensity measures for near-source and ordinary earthquake ground motions. Earthq Spectra 23(2):357–392

Mavroeidis GP, Papageorgiou AS (2003) A mathematical representation of near-fault ground motions. Bull Seismol Soc Am 93(3):1099–1131

Mazzoni S, McKenna F, Scott MH, Fenves GL (2006) OpenSees command language manual. Pac Earthq Eng Research (PEER) Cent 264(1):137–158

McGuire RK (2007) Probabilistic seismic hazard analysis: Early history. Earthq Eng Struct Dyn 37(3):329–338

McGuire RK (2004) Seismic hazard and risk analysis. Earthquake Engineering Research Institute

McGuire RK (1995) Probabilistic seismic hazard analysis and design earthquakes: closing the loop. Bull Seismol Soc Am 85(5):1275–1284

Mehanny SS (2009) A broad-range power-law form scalar-based seismic intensity measure. Eng Struct 31(7):1354–1368

Mousavi M, Ghafory-Ashtiany M, Azarbakht A (2011) A new indicator of elastic spectral shape for the reliable selection of ground motion records. Earthq Eng Struct Dyn 40(12):1403–1416

Musson RMW, Sargeant SL (2007) Eurocode 8 seismic hazard zoning maps for the UK. Technical Report CR/07/125, issue no. 3, British Geological Survey

O'Reilly GJ (2021) Seismic intensity measures for risk assessment of bridges. Bull Earthq Eng 19(9):3671–3699

Rodriguez-Marek A, Cotton F, Abrahamson NA, Akkar S, Al Atik L, Edwards B, Montalva GA, Dawood HM (2013) A model for single-station standard deviation using data from various tectonic regions. Bull Seismol Soc Am 103(6):3149–3163

Somerville PG, Smith NF, Graves RW, Abrahamson NA (1997) Modification of empirical strong ground motion attenuation relations to include the amplitude and duration effects of rupture directivity. Seismol Res Lett 68(1):199–222

Sotolongo-Costa O, Posadas A (2004) Fragment-asperity interaction model for earthquakes. Phys Rev Lett 92(4):048501

Schwartz DP, Coppersmith KJ (1984) Fault behavior and characteristic earthquakes: examples from the Wasatch and San Andreas fault zones. J Geophys Res Solid Earth 89(B7):5681–5698

Takeda T, Sozen MA, Nilsen NN (1970) Reinforced concrete response to simulated earthquakes. J Struct Div 96(12):2557–2573

Tothong P, Luco N (2007) Probabilistic seismic demand analysis using advanced ground motion intensity measures. Earthq Eng Struct Dyn 36(13):1837–1860

Vamvatsikos D, Cornell CA (2002) Incremental dynamic analysis. Earthq Eng Struct Dyn 31(3):491–514

Vargas-Alzate YF, Hurtado JE, Pujades LG (2022) New insights into the relationship between seismic intensity measures and nonlinear structural response. Bull Earthq Eng. https://doi.org/10.1007/s10518-021-01283-

Wesnousky SG (1994) The Gutenberg-Richter or characteristic earthquake distribution, which is it? Bull Seismol Soc Am 84(6):1940–1959

Authors and Affiliations

Alireza Azarbakht[1]

✉ Alireza Azarbakht
A.Azarbakht@greenwich.ac.uk

[1] School of Engineering, University of Greenwich, Medway Campus, Chatham ME4 4TB, UK